Anisotropic magnetocapacitance of antiferromagnetic cycloids in BiFeO3

Maximilian Winkler, Korbinian Geirhos, Tobias Tyborowski, Boglarka Toth, D. G. Farkas, Jonathan White, Toshimitsu Ito, Stephan Krohns, Peter Lunkenheimer, Sandor Bordacs, István Kézsmárki

Angaben zur Veröffentlichung / Publication details:

Winkler, Maximilian, Korbinian Geirhos, Tobias Tyborowski, Boglarka Toth, D. G. Farkas, Jonathan White, Toshimitsu Ito, et al. 2024. "Anisotropic magnetocapacitance of antiferromagnetic cycloids in BiFeO3." Applied Physics Letters 125 (25): 252902. https://doi.org/10.1063/5.0237659.

RESEARCH ARTICLE | DECEMBER 16 2024

Anisotropic magnetocapacitance of antiferromagnetic cycloids in $BiFeO_3$

M. Winkler ; K. Geirhos ; T. Tyborowski ; B. Tóth ; D. G. Farkas; J. S. White ; T. Ito ; S. Krohns ; P. Lunkenheimer ; S. Bordács ; I. Kézsmárki

Appl. Phys. Lett. 125, 252902 (2024)
https://doi.org/10.1063/5.0237659

Applied Physics Letters ARTICLE pubs.aip.org/aip/apl

Anisotropic magnetocapacitance of antiferromagnetic cycloids in $BiFeO_3$

Cite as: Appl. Phys. Lett. **125**, 252902 (2024); doi: 10.1063/5.0237659
Submitted: 6 September 2024 · Accepted: 28 November 2024 ·
Published Online: 16 December 2024

M. Winkler,[1,a)] K. Geirhos,[1] T. Tyborowski,[1] B. Tóth,[2] D. G. Farkas,[2] J. S. White,[3] T. Ito,[4] S. Krohns,[1] P. Lunkenheimer,[1] S. Bordács,[1,2,5] and I. Kézsmárki[1]

AFFILIATIONS

[1]Experimental Physics V, Center for Electronic Correlations and Magnetism, University of Augsburg, 86135 Augsburg, Germany
[2]Department of Physics, Institute of Physics, Budapest University of Technology and Economics, Műegyetem rkp. 3., H-1111 Budapest, Hungary
[3]Laboratory for Neutron Scattering and Imaging (LNS), PSI Center for Neutron and Muon Sciences, Paul Scherrer Institute, CH-5232 Villigen, Switzerland
[4]National Institute of Advanced Industrial Science and Technology (AIST), Tsukuba, 305-8562 Ibaraki, Japan
[5]HUN-REN–BME Condensed Matter Physics Research Group, Budapest University of Technology and Economics, Műegyetem rkp. 3., H-1111 Budapest, Hungary

[a)]**Author to whom correspondence should be addressed:** maximilian.winkler@physik.uni-augsburg.de

ABSTRACT

Distinguishing different antiferromagnetic domains by electrical probes is a challenging task, which in itinerant compounds can be achieved, e.g., via the anisotropic magnetoresistance. Here, we demonstrate that in insulators, the anisotropic magnetocapacitance can be exploited for the same purpose. We studied the magnetic field dependence of the dielectric response in $BiFeO_3$, one of the few room-temperature multiferroics. We observed a sizeable dielectric anisotropy upon the rotation of the modulation vector of the antiferromagnetic cycloid in the plane normal to the rhombohedral axis. Importantly, this anisotropy is characteristic of the cycloidal mono-domain state even in zero magnetic field, thus facilitating the determination of the antiferromagnetic domain population. This approach can be utilized to electrically distinguish between antiferromagnetic domains even in complex magnets, such as modulated spin structures, via the magnetodielectric coupling.

The application of magnetic materials beyond ferro- and ferrimagnets in data storage and logic devices has been motivating intense research to find novel ways to detect domains of compensated spin structures.[1–3] Although advanced scattering and imaging techniques provide a detailed description of the magnetic order, simpler, low-cost, scalable electric probes are more applicable in real devices. For example, in itinerant magnets, the measurement of the anisotropic magnetoresistance (AMR) allows the readout of the orientation of the antiferromagnetic (AFM) state with respect to the current direction.[2,3] In insulators, where a direct current cannot flow, this goal may be achieved via the magnetoelectric effect or the magnetocapacitance, namely, by detecting the magnetic field-induced electric polarization or dielectric permittivity, respectively,.[4–11] In magnetoelectric multiferroics, these weak effects are usually enhanced due to the coexistence of ferroelectricity and magnetic order. In fact, sizeable magnetocapacitance has been reported in prototypical multiferroics such as $TbMnO_3$ and $BiMnO_3$.[6,7] However, their magnetically ordered phase emerges only at low temperatures hindering their applications.

Here, we report a systematic magnetocapacitance study in $BiFeO_3$, one of the few room-temperature multiferroics. The ferroelectric polarization of $BiFeO_3$ emerges below ~ 1100 K along with one of the $\langle 111 \rangle$ directions of the cubic perovskite structure.[12–17] In the following, we refer to the crystallographic axes $[1\bar{1}0]$, $[11\bar{2}]$, and [111] as **X**, **Y**, and **Z**, respectively, where **Z** is parallel to the ferroelectric polarization.[18] Within the ferroelectric phase, a G-type AFM order develops below $T_N = 640$ K,[19] thus, $BiFeO_3$ becomes multiferroic far above room temperature.[20–23] Moreover, its ferroelectric and magnetic orders are not independent. The corresponding magnetoelectric coupling is manifested both in the static magnetically induced polarization[24,25] and in the non-reciprocal absorption of spin waves due to the dynamic magnetoelectric effect.[26–29] The ferroelectric distortion via the Dzyaloshinskii–Moriya interaction leads to a long-wavelength cycloidal

modulation of the AFM order, i.e., the spins rotate in the plane spanned by the ferroelectric polarization and the propagation vector q of the modulation.[12,30] This contrasts with the short-period cycloids of $TbMnO_3$ stabilized by magnetic frustration.[31]

In $TbMnO_3$, the plane of cycloids flops suddenly above a critical magnetic field, which is observable in the magnetic field dependence of the dielectric constant as a distinct peak.[6] In contrast, the cycloidal modulation vector in $BiFeO_3$ can be smoothly rotated about the rhombohedral **Z** axis by moderate magnetic fields, as revealed by small angle neutron scattering (SANS) and THz spectroscopy.[29,32] A similar rotation of the cycloidal q vectors about the trigonal axis by weak magnetic fields has been reported for ferromagnetic cycloids in Néel-type skyrmion hosts GaV_4S_8[33] and GaV_4Se_8.[34,35] In zero field, a weak magnetic anisotropy pins the orientations of **q** in the ⟨110⟩-type directions as shown in Fig. 1(a). In a magnetic field, **H** the q vectors tend to rotate within the XY plane to be perpendicular to the field: the field applied along **H** ∥ **X** and **H** ∥ **Y** rotates the q vectors to the **q** ∥ **Y** and **q** ∥ **X** directions, respectively, as shown in Figs. 1(b) and 1(c).

In this Letter, we demonstrate that dielectric anisotropy provides a sensitive probe to detect the orientation of the cycloidal q vectors in $BiFeO_3$. Our study reveals that the dielectric constant is either decreasing or increasing in decreasing magnetic fields applied along or perpendicular to **q**, respectively. We find that the dielectric response is sensitive to the orientation of the cycloidal q vector and thus can be used to trace its variations. We characterized the field-induced changes by rotating the magnetic field in the XY plane and modeling the measured dielectric anisotropy. This anisotropy is characteristic of the cycloidal mono-domain state even in a zero magnetic field; therefore, it originates from the cycloidal magnetic order.

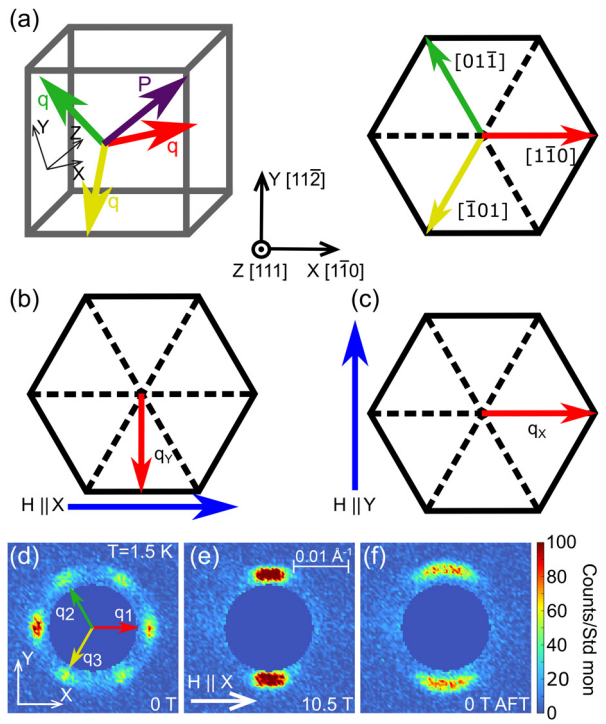

FIG. 1. (a) Schematic representation of the parent cubic unit cell. The arrows indicate the direction of the polarization **P** and the direction of **q** in zero fields. The arrows in the hexagonal plane indicate three directions of **q** favored in zero magnetic fields. (b) and (c) depict the **q** alignments after applying magnetic fields, respectively, along the X and Y directions. The directions are given in the cubic reference. (d)–(f) SANS images measured at 1.5 K. (d) shows the zero-field cooled state with **q** vectors parallel to **X**-type directions. (e) A magnetic field of 10.5,T applied along **X** rotates the **q** vectors to the perpendicular **Y** direction, and (f) depicts the remanent zero-field state after the field treatment (AFT).

High-quality ferroelectric monodomain single crystals were grown using the laser–diode heating floating-zone method as reported in Ref. 16. To enable measurements of all diagonal components of the dielectric tensor, we cut slabs from the single crystal rod with plane-parallel surfaces perpendicular to the X, Y, and Z directions. We established a capacitor-like geometry by painting these surfaces with conducting silver paste, which we connected to a Novocontrol α-Analyzer or an Andeen-Hagerling AH2700-A capacitance bridge to measure the dielectric constant at 10 kHz. We carried out the measurements in an Oxford helium cryostat with a superconducting magnet providing a magnetic field of up to 14 T in a temperature range between 2 and 300 K. We used a rotatable sample holder equipped with two coaxial cables connecting the sample to measure the angular dependence of the static field and the oscillating electric field.

SANS experiments were carried out on a 25-mg ferroelectric monodomain $BiFeO_3$ single crystal. Measurements were performed using the SANS-I instrument at Paul Scherrer Institut. The incoming neutron wavelength was set to 8 Å, and the instrument collimation length and the sample-to-detector distance were both 15 m. The low-temperature sample environment and magnetic fields up to 11 T were provided by an Oxford cryomagnet (MA11). The SANS measurements were done by tilting and rotating the sample and cryomagnet together through angular ranges (rocking angles) that moved the magnetic diffraction peaks through the Ewald sphere.

We carried out additional SANS experiments besides the results published in Ref. 32. Figures 1(d)–1(f) show typical SANS images captured at 1.5 K, which are the sum of detector images recorded at each rocking angle with an incoming neutron beam nearly parallel to **Z**. After zero-field cooling the sample from above T_N, the detector image in Fig. 1(d) displays six distinct Bragg spots implying q vectors pointing to the **X**-type directions. The three pairs of the q vectors: $\mathbf{q}_1$, $\mathbf{q}_2$, and $\mathbf{q}_3$ [colored arrows in Fig. 1(d)] correspond to the three cycloidal domains. The nearly equal intensity suggests a homogeneous distribution of domains over the three possible states. Applying a magnetic field along **X** leads to a rearrangement of the cycloidal domains. In 10.5 T, q vectors are distributed in the close vicinity of the Y direction, perpendicular to the field, as illustrated in Fig. 1(e). After decreasing the field to zero again, the q vectors remain at the high-field positions, as shown in Fig. 1(f), with only the spots slightly spread in the polar directions. This pattern remains stable even after heating the crystal to room temperature.[32]

We now turn to the discussion of the magnetic-field-induced changes in the dielectric constant, $\Delta\varepsilon'$. We performed all experiments at 100 K to ensure the detection of purely intrinsic behavior, as the extrinsic Maxwell–Wagner relaxation,[36,37] for a single crystal with silver-paint contacts, at 10 kHz occurs above 250 K only (see the supplementary material, Fig. S1).[23] We measured the diagonal components of $\Delta\varepsilon'$ with probing AC electric field, $\mathbf{E}^{\omega}$ parallel to the **X**, **Y**, and **Z** axes, as depicted in Figs. 2(a)–2(c), respectively. Before the experiments, we applied a magnetic field of 14 T along the Y direction.

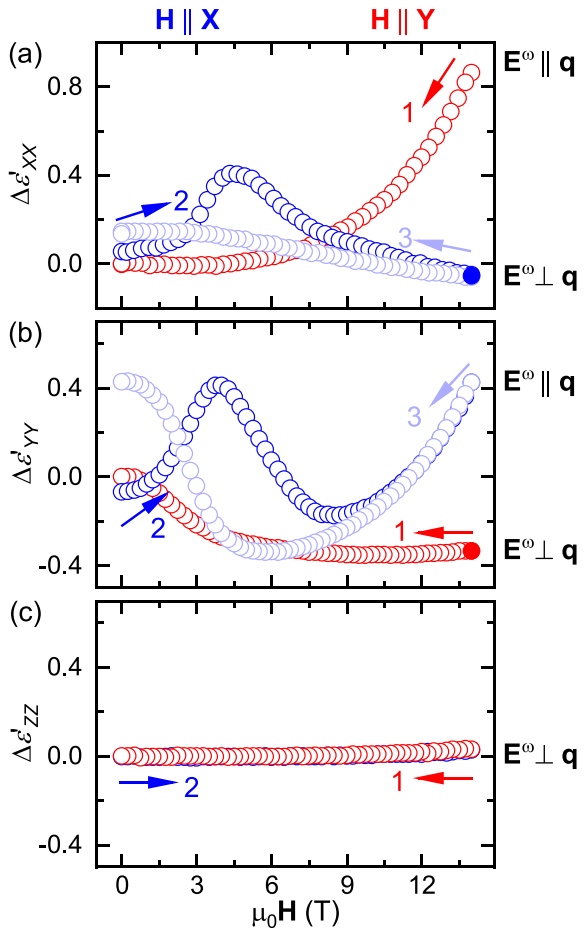

FIG. 2. Magnetic field-dependent change of the *XX* (a), *YY* (b), and *ZZ* component (c) of the dielectric constant at 100 K and 10 kHz for the probing electric field $\mathbf{E}^{\omega} \parallel \mathbf{X}, \mathbf{Y}, \mathbf{Z}$, respectively. The direction of the magnetic field is indicated by the color code on top of the figure. For all red points, the magnetic field is parallel to **Y**, and the magnetic field is along **X** in case of the light blue and blue points. In all cases, we start ramping down the magnetic field applied along the *Y* direction (red) and then proceed with the application of the magnetic field along **X** (blue). Subsequently, we decrease the magnetic field along **X** (light blue). On the right hand side of each panel, the electric field orientation is also given with respect to the *q* vector aligned by high magnetic fields.

According to the SANS experiments, this field was sufficient to orient the cycloidal q vectors perpendicular to the field, i.e., $\mathbf{q} \parallel \mathbf{X}$. First, we measured the dielectric response in decreasing fields $\mathbf{H} \parallel \mathbf{Y}$ (red symbols). After reaching zero field, we set $\Delta\varepsilon' = 0$ for all directions. Then we rotated the sample stage by 90°, applied the magnetic field in the orthogonal direction, $\mathbf{H} \parallel \mathbf{X}$, and increased it up to 14 T (blue symbols). The slight difference between the zero-field values (compare red and blue symbols in zero-field) is due to the slight twisting of the cables. Finally, we decreased the field back to 0 T (light blue symbols) while measuring the change in the dielectric constant.

In high magnetic fields, the in-plane dielectric response is clearly sensitive to the orientation of the cycloidal propagation vector **q** [see Figs. 2(a) and 2(b)]. Irrespective of the field history, we observed a positive magnetocapacitive effect at the highest magnetic fields for $\mathbf{E}^{\omega} \parallel \mathbf{q}$. In contrast, if $\mathbf{E}^{\omega} \perp \mathbf{q}$, there is a negative magnetocapacitance. The large q vector-dependent difference, $\Delta\varepsilon' \sim 0.8$ is the same for both $\Delta\varepsilon'_{\mathbf{XX}}$ and $\Delta\varepsilon'_{\mathbf{YY}}$. When the magnetic field direction is rotated after high fields, the blue curves in (a) and (b) exhibit a broad peak at ∼4 T. In small increasing magnetic fields, the q vectors are still parallel to the field, thus, they need to rotate over large volumes. At this reorientation transition, smaller cycloidal domains should appear responsible for the enhanced dielectric response. When the field is decreased to zero again, there is a finite difference for $\mathbf{H} \parallel \mathbf{Y}$ and $\mathbf{H} \parallel \mathbf{X}$—see and compare light blue and red symbols in Fig. 2(a) as well as in Fig. 2(b). This zero-field anisotropy suggests that dielectric spectroscopy is capable of detecting the orientation of the cycloidal **q** vectors. In contrast to high fields, this zero-field dielectric contrast depends on the crystallographic orientation. The rotation of the cycloidal structure leads to different zero-field responses when probed by $\mathbf{E}^{\omega} \parallel \mathbf{X}$ and $\mathbf{E}^{\omega} \parallel \mathbf{Y}$. In contrast to the in-plane dielectric response, the dielectric constant measured with electric fields oscillating along the ferroelectric polarization, $\Delta\varepsilon'_{ZZ}$ remains featureless and constant, irrespective of the direction of the applied magnetic field, as shown in Fig. 2(c).

Next, we studied the high-field magnetocapacitance anisotropy by measuring the dielectric response for $\mathbf{E}^{\omega} \parallel \mathbf{X}$ and $\mathbf{E}^{\omega} \parallel \mathbf{Y}$ separately while rotating a magnetic field in the plane normal to the Z axis. The results are displayed in Fig. 3, where the angle of the field, ϕ is measured from the X axis. As a first step, we applied the highest magnetic field of 14 T along the X axis, which forced the **q** vector to be perpendicular, thus, $\mathbf{q} \parallel \mathbf{Y}$, and measured $\Delta\varepsilon'_{XX}$, as depicted in Fig. 3(a). The starting point indicated as the blue circle at 0° corresponds to the value obtained from Fig. 2(a) for the case $\mathbf{E}^{\omega} \perp \mathbf{q}$ at 14 T. As the field is rotated, the cycloids tend to maintain their relative orientation, thus, at 90° the q vectors point to the X direction, and they become parallel to the oscillating electric field, $\mathbf{E}^{\omega} \parallel \mathbf{q}$. By a further 90° rotation, the oscillating electric field probes the $\mathbf{E}^{\omega} \perp \mathbf{q}$ state again. $\Delta\varepsilon'$ is the largest near $\mathbf{E}^{\omega} \parallel \mathbf{q}$ and has the smallest value at $\mathbf{E}^{\omega} \perp \mathbf{q}$, in agreement with the field-dependent experiments presented in Fig. 2. The angular dependence of $\Delta\varepsilon'_{YY}$ is shown in Fig. 3(b). To better compare the relative orientation of the oscillating electric field and the q vector to the previous case [Fig. 3(a)], the angular scale is shifted by 90°. Here, in the initially probed state, the q vector is pointing in the X direction ($\mathbf{E}^{\omega} \perp \mathbf{q}$), and the starting point, indicated in red, corresponds to the value obtained in Fig. 2(b). In agreement with Fig. 2, $\Delta\varepsilon'$ distinguishes between the parallel and perpendicular orientation of the cycloidal q vector with respect to the oscillating electric field. However, we observed two distinct maxima at 60° and 120°, and a local minimum at 90°. The maxima occur when the q vector is parallel with one of the six symmetry equivalent X directions. As these are the equilibrium positions in zero-field (see Fig. 1), the cycloids tend to pin to those. Accordingly, at 90° not all the cycloids are perfectly aligned perpendicular to the field.

In order to describe the field angle dependence of the dielectric constant shown in Fig. 3, we developed a model ascribing the dielectric anisotropy to the presence of spin cycloids. In the XY plane, the applied AC electric field, $\mathbf{E}^{\omega}$ induces a displacement field, $\mathbf{D}^{\omega} = \hat{\varepsilon}\mathbf{E}^{\omega}$. Without the magnetic order, this plane is isotropic and the dielectric tensor, $\hat{\varepsilon}$ is proportional to the unit tensor due to the

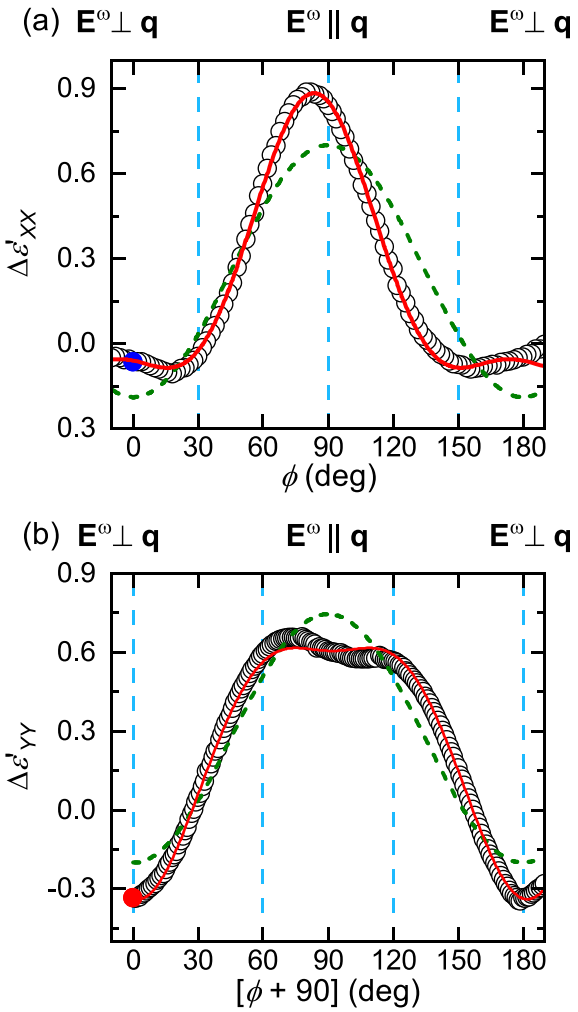

FIG. 3. Change of the *XX* (a) and *YY* component (b) of the dielectric constant at 100 K and 10 kHz for cycloidal **q** vector rotated in the *XY* plane by a magnetic field of 14 T. 0°/90° correspond to **q** oriented perpendicular/parallel to the direction along which the dielectric constant was measured ($\mathbf{E}^{\omega} \perp \mathbf{q}/\mathbf{E}^{\omega} \parallel \mathbf{q}$). The blue dashed vertical lines indicate the inherently zero field directions of the **q** vector. The models used in the fits represented by green, orange, and red lines are described in the text. The starting points, indicated in red and blue, correspond to Fig. 2.

C_{3v} symmetry of the ferroelectric phase. The spin cycloid breaks this symmetry and allows an anisotropic dielectric response. For the sake of simplicity, we assume that in the coordinate system attached to the cycloid the dielectric tensor is diagonal, and merely the components induced by an in-plane field parallel and perpendicular to **q**, $\varepsilon_{\parallel \mathbf{q}}$, and $\varepsilon_{\perp \mathbf{q}}$, respectively, are different

$$\mathbf{D}^{\omega} = \begin{bmatrix} \varepsilon_{\parallel \mathbf{q}} & 0 \\ 0 & \varepsilon_{\perp \mathbf{q}} \end{bmatrix} \mathbf{E}^{\omega}. \tag{1}$$

Since the displacement parallel to the excitation electric field is probed in our experiment, the measured dielectric function can be deduced by a projection

$$\begin{aligned} \varepsilon' &= \varepsilon_{\parallel \mathbf{q}} \cos^2(\alpha) + \varepsilon_{\perp \mathbf{q}} \sin^2(\alpha) \\ &= \frac{\varepsilon_{\parallel \mathbf{q}} + \varepsilon_{\perp \mathbf{q}}}{2} + \frac{\varepsilon_{\parallel \mathbf{q}} - \varepsilon_{\perp \mathbf{q}}}{2} \cos(2\alpha), \end{aligned} \tag{2}$$

where α is the angle spanned by the q vector and the electric field.

By assuming that in high magnetic fields, the q vector is perpendicular to the magnetic field (see Fig. 1), the dielectric function can be deduced as a function of the field angle ϕ, measured from the X axis: $\alpha = \phi + \frac{\pi}{2}$ for ε'_{XX}, whereas, $\alpha = \phi$ for ε'_{YY}. Fitting the measured data using this model, we obtain the green dashed lines in Fig. 3.

This simplistic model can be made more realistic by adding a $\sin(6\phi)$ term to α to take into account that the q vectors are not strictly perpendicular to the magnetic field due to the sixfold magnetocrystalline anisotropy in the XY plane. Furthermore, the distribution of the q vectors has some broadening even in finite magnetic fields as displayed Fig. 1e (see the elongation of the spots along the **X** axis). For simplicity, we mimic the broadening of the distribution by shifting the angular dependence by $\pm d\phi$ and averaging them. Then, we obtain

$$\begin{aligned} \varepsilon'_{XX/YY}(\phi) = \frac{\varepsilon_{\parallel \mathbf{q}} + \varepsilon_{\perp \mathbf{q}}}{2} - / + \frac{\varepsilon_{\parallel \mathbf{q}} - \varepsilon_{\perp \mathbf{q}}}{2} \Bigg(\frac{\cos(2\phi_+) + \cos(2\phi_-)}{2} \\ + c \sin(2\phi_+) \sin(6\phi_+) + c \sin(2\phi_-) \sin(6\phi_-) \Bigg) \end{aligned} \tag{3}$$

The full derivation is shown in the supplementary material.

This model reasonably fits the data as shown by the red lines in Fig. 3. The parameters obtained from the fits of ε'_{XX} and ε'_{YY} (shown in Table I) are close to each other, which confirms those intrinsic properties of the material. The positive c parameter indicates that the q vector prefers pointing parallel to **X**. This and the $d\phi \sim 11°$ spread of the q vector distribution are in agreement with former neutron scattering results, as the full width at half maximum (FWHM) of the high-field angular distribution of the scattering data [see Fig. 1(e)] is $\sim 25.6°$ (Table I).

In conclusion, we observed magnetocapacitance anisotropy in $BiFeO_3$ induced by its AFM cycloid structure. We found positive and negative magnetocapacitance when measuring with electric fields oscillating parallel and perpendicular to the cycloid propagation vector, respectively. By rotating a magnetic field in the plane perpendicular to the rhombohedral axis, we examined the angular dependence of the dielectric constant. Assuming a distribution of cycloidal domains having anisotropic dielectric response, we developed a model that captures this angular dependence. With these experiments, we demonstrated that anisotropic magnetocapacitance offers a simple and accessible electrical method for determining the orientation of cycloidal modulation vector, without the need to perform scattering experiments. This approach holds promise for broader data-storage applications in

TABLE I. Fit parameters used to reproduce the angular dependence of the dielectric response shown in Fig. 3.

	ε'_{XX} shown in Fig. 3(a)	ε'_{YY} shown in Fig. 3(b)
$\varepsilon_{\parallel \mathbf{q}}$	0.75 (6)	0.78 (5)
$\varepsilon_{\perp \mathbf{q}}$	−0.26 (1)	−0.23 (9)
c	0.45 (7)	0.37 (9)
$d\phi$	11.3 (1)°	11.4 (0)°

detecting the orientation of compensated magnetic structures in a wide range of magnets.

See the supplementary material for the absolute values of the temperature-dependent real part of the dielectric constant for several frequencies with $\mathbf{E}^{\omega}$ along **X**, **Y**, and **Z**.

This work was supported by the Deutsche Forschungsgemeinschaft (DFG) through Transregional Research Collaboration TRR 360 (project No. 492547816) and DFG Grant No. KE 2370/3-1 (project No. 437124857) and by the Hungarian National Research, Development and Innovation Office via NKFIH Grant No. FK 135003. This research was supported by the Ministry of Culture and Innovation and the National Research, Development, and Innovation Office within the Quantum Information National Laboratory of Hungary (Grant No. 2022-2.1.1-NL-2022-00004). This work is based partly on experiments performed at the Swiss Spallation Neutron Source SINQ, Paul Scherrer Institute, Villigen, Switzerland.

AUTHOR DECLARATIONS

Conflict of Interest

The authors have no conflicts to disclose.

Author Contributions

M. Winkler: Conceptualization (equal); Formal analysis (equal); Investigation (equal); Methodology (equal); Writing – original draft (equal); Writing – review & editing (equal). **K. Geirhos:** Formal analysis (equal); Investigation (equal). **T. Tyborowski:** Formal analysis (equal); Investigation (equal). **B. Tóth:** Formal analysis (equal); Investigation (equal); Writing – review & editing (equal). **D. G. Farkas:** Formal analysis (equal); Investigation (equal). **J. S. White:** Formal analysis (equal); Investigation (equal). **T. Ito:** Formal analysis (equal); Investigation (equal). **S. Krohns:** Supervision (equal). **P. Lunkenheimer:** Formal analysis (equal). **S. Bordács:** Conceptualization (equal); Formal analysis (equal); Supervision (equal); Writing – review & editing (equal). **I. Kézsmárki:** Conceptualization (equal); Supervision (equal).

DATA AVAILABILITY

The data that support the findings of this study are available from the corresponding author upon reasonable request.

REFERENCES

[1]P. Wadley, B. Howells, J. Železný, C. Andrews, V. Hills, R. P. Campion, V. Novák, K. Olejník, F. Maccherozzi, S. S. Dhesi, S. Y. Martin, T. Wagner, J. Wunderlich, F. Freimuth, Y. Mokrousov, J. Kuneš, J. S. Chauhan, M. J. Grzybowski, A. W. Rushforth, K. W. Edmonds, B. L. Gallagher, and T. Jungwirth, "Electrical switching of an antiferromagnet," Science **351**, 587–590 (2016).
[2]T. Jungwirth, X. Marti, P. Wadley, and J. Wunderlich, "Antiferromagnetic spintronics," Nat. Nanotechol. **11**, 231–241 (2016).
[3]V. Baltz, A. Manchon, M. Tsoi, T. Moriyama, T. Ono, and Y. Tserkovnyak, "Antiferromagnetic spintronics," Rev. Mod. Phys. **90**, 015005 (2018).
[4]D. Astrov, "The magnetoelectric effect in antiferromagnetics," Sov. Phys. JETP **38**, 984–985 (1960).
[5]M. Fiebig, "Revival of the magnetoelectric effect," J. Phys. D: Appl. Phys. **38**, R123 (2005).
[6]T. Kimura, T. Goto, H. Shintani, K. Ishizaka, T. Arima, and Y. Tokura, "Magnetic control of ferroelectric polarization," Nature **426**, 55–58 (2003).
[7]T. Kimura, S. Kawamoto, I. Yamada, M. Azuma, M. Takano, and Y. Tokura, "Magnetocapacitance effect in multiferroic $BiMnO_3$," Phys. Rev. B **67**, 180401 (2003).
[8]J. Hemberger, P. Lunkenheimer, R. Fichtl, H.-A. Krug von Nidda, V. Tsurkan, and A. Loidl, "Relaxor ferroelectricity and colossal magnetocapacitive coupling in ferromagnetic $CdCr_2S_4$," Nature **434**, 364–367 (2005).
[9]S. Weber, P. Lunkenheimer, R. Fichtl, J. Hemberger, V. Tsurkan, and A. Loidl, "Colossal magnetocapacitance and colossal magnetoresistance in $HgCr_2S_4$," Phys. Rev. Lett. **96**, 157202 (2006).
[10]G. Catalan, "Magnetocapacitance without magnetoelectric coupling," Appl. Phys. Lett. **88**, 102902 (2006).
[11]J.-S. Jung, A. Iyama, H. Nakamura, M. Mizumaki, N. Kawamura, Y. Wakabayashi, and T. Kimura, "Magnetocapacitive effects in the Néel N-type ferrimagnet $SmMnO_3$," Phys. Rev. B **82**, 212403 (2010).
[12]I. Sosnowska, T. P. Neumaier, and E. Steichele, "Spiral magnetic ordering in bismuth ferrite," J. Phys. C: Solid State Phys. **15**, 4835 (1982).
[13]J. Wang, J. B. Neaton, H. Zheng, V. Nagarajan, S. B. Ogale, B. Liu, D. Viehland, V. Vaithyanathan, D. G. Schlom, U. V. Waghmare, N. A. Spaldin, K. M. Rabe, M. Wuttig, and R. Ramesh, "Epitaxial $BiFeO_3$ multiferroic thin film heterostructures," Science **299**, 1719–1722 (2003).
[14]D. Lebeugle, D. Colson, A. Forget, M. Viret, P. Bonville, J. F. Marucco, and S. Fusil, "Room-temperature coexistence of large electric polarization and magnetic order in $BiFeO_3$ single crystals," Phys. Rev. B **76**, 024116 (2007).
[15]S. Lee, T. Choi, W. Ratcliff, R. Erwin, S.-W. Cheong, and V. Kiryukhin, "Single ferroelectric and chiral magnetic domain of single-crystalline $BiFeO_3$ in an electric field," Phys. Rev. B **78**, 100101 (2008).
[16]T. Ito, T. Ushiyama, Y. Yanagisawa, R. Kumai, and Y. Tomioka, "Growth of highly insulating bulk single crystals of multiferroic $BiFeO_3$ and their inherent internal strains in the domain-switching process," Cryst. Growth Des. **11**, 5139–5143 (2011).
[17]S. Krohns and P. Lunkenheimer, "Ferroelectric polarization in multiferroics," Phys. Sci. Rev. **4**, 20190015 (2019).
[18]Throughout the text, we are using the pseudo-cubic notation.
[19]S. V. Kiselev, R. P. Ozerov, and G. S. Zhdanov, "Detection of magnetic order in ferroelectric $BiFeO_3$ by neutron diffraction," Sov. Phys. Dokl. **7**, 742 (1963).
[20]Y. E. Roginskaya, Y. Y. Tomashpol'Skiĭ, Y. N. Venevtsev, V. M. Petrov, and G. S. Zhdanov, "The nature of the dielectric and magnetic properties of $BiFeO_3$," Sov. Phys. JETP **23**, 47 (1966).
[21]P. Fischer, M. Polomska, I. Sosnowska, and M. Szymanski, "Temperature dependence of the crystal and magnetic structures of $BiFeO_3$," J. Phys. C: Solid State Phys. **13**, 1931 (1980).
[22]C. Ederer and N. A. Spaldin, "Weak ferromagnetism and magnetoelectric coupling in bismuth ferrite," Phys. Rev. B **71**, 060401 (2005).
[23]J. Lu, A. Günther, F. Schrettle, F. Mayr, S. Krohns, P. Lunkenheimer, A. Pimenov, V. D. Travkin, A. A. Mukhin, and A. Loidl, "On the room temperature multiferroic $BiFeO_3$: Magnetic, dielectric and thermal properties," Eur. Phys. J. B **75**, 451–460 (2010).
[24]S. Kawachi, S. Miyahara, T. Ito, A. Miyake, N. Furukawa, J-i Yamaura, and M. Tokunaga, "Direct coupling of ferromagnetic moment and ferroelectric polarization in $BiFeO_3$," Phys. Rev. B **100**, 140412 (2019).
[25]M. Tokunaga, M. Akaki, T. Ito, S. Miyahara, A. Miyake, H. Kuwahara, and N. Furukawa, "Magnetic control of transverse electric polarization in $BiFeO_3$," Nat. Commun. **6**, 5878 (2015).
[26]I. Kézsmárki, U. Nagel, S. Bordács, R. S. Fishman, J. H. Lee, H. T. Yi, S.-W. Cheong, and T. Rõõm, "Optical diode effect at spin-wave excitations of the room-temperature multiferroic $BiFeO_3$," Phys. Rev. Lett. **115**, 127203 (2015).
[27]R. S. Fishman, J. H. Lee, S. Bordács, I. Kézsmárki, U. Nagel, and T. Rõõm, "Spin-induced polarizations and nonreciprocal directional dichroism of the room-temperature multiferroic $BiFeO_3$," Phys. Rev. B **92**, 094422 (2015).
[28]B. Tóth, D. G. Farkas, K. Amelin, T. Rõõm, U. Nagel, L. Udvardi, L. Szunyogh, L. Rózsa, T. Ito, and S. Bordács, "Terahertz spin-wave excitations in the transverse conical phase of $BiFeO_3$," Phys. Rev. B **109**, 144424 (2024).
[29]D. G. Farkas, D. Szaller, I. Kézsmárki, U. Nagel, T. Rõ om, L. Peedu, J. Viirok, J. S. White, R. Cubitt, T. Ito, R. S. Fishman, and S. Bordács, "Selection rules and dynamic magnetoelectric effect of the spin waves in multiferroic $BiFeO_3$," Phys. Rev. B **104**, 174429 (2021).
[30]D. Lebeugle, D. Colson, A. Forget, M. Viret, A. M. Bataille, and A. Gukasov, "Electric-field-induced spin flop in $BiFeO_3$ single crystals at room temperature," Phys. Rev. Lett. **100**, 227602 (2008).

[31]S. Quezel, F. Tcheou, J. Rossat-Mignod, G. Quezel, and E. Roudaut, "Magnetic structure of the perovskite-like compound $TbMnO_3$," Phys. B+C **86–88**, 916–918 (1977).
[32]S. Bordács, D. G. Farkas, J. S. White, R. Cubitt, L. DeBeer-Schmitt, T. Ito, and I. Kézsmárki, "Magnetic field control of cycloidal domains and electric polarization in multiferroic $BiFeO_3$," Phys. Rev. Lett. **120**, 147203 (2018).
[33]J. S. White, A. Butykai, R. Cubitt, D. Honecker, C. D. Dewhurst, L. F. Kiss, V. Tsurkan, and S. Bordács, "Direct evidence for cycloidal modulations in the thermal-fluctuation-stabilized spin spiral and skyrmion states of GaV_4S_8," Phys. Rev. B **97**, 020401 (2018).
[34]S. Bordács, A. Butykai, B. G. Szigeti, J. S. White, R. Cubitt, A. O. Leonov, S. Widmann, D. Ehlers, H.-A. K. von Nidda, V. Tsurkan, A. Loidl, and I. Kézsmárki, "Equilibrium skyrmion lattice ground state in a polar easy-plane magnet," Sci. Rep. **7**, 7584 (2017).
[35]K. Geirhos, B. Gross, B. G. Szigeti, A. Mehlin, S. Philipp, J. S. White, R. Cubitt, S. Widmann, S. Ghara, P. Lunkenheimer, V. Tsurkan, E. Neuber, D. Ivaneyko, P. Milde, L. M. Eng, A. O. Leonov, S. Bordács, M. Poggio, and I. Kézsmárki, "Macroscopic manifestation of domain-wall magnetism and magnetoelectric effect in a Néel-type skyrmion host," npj Quantum Mater. **5**, 44 (2020).
[36]J. C. Maxwell, *Treatise on Electricity and Magnetism*, edited by J. C. Maxwell (Dover Publications, New York, 1970), Vol. 1, p. 519.
[37]P. Lunkenheimer, V. Bobnar, A. V. Pronin, A. I. Ritus, A. A. Volkov, and A. Loidl, "Origin of apparent colossal dielectric constants," Phys. Rev. B **66**, 052105 (2002).